FORM TI-12
07/1999

B-T-3228

DRY PATCH STABILITY OF SHEAR DRIVEN LIQUID FILM

D. G. Penn
M. L. de Bertodano
P. Lykoudis
Purdue University

S. G. Beus

DE-AC11-98PN38206

BETTIS ATOMIC POWER LABORATORY WEST MIFFLIN, PENNSYLVANIA 15122-0079

Operated for the U.S. Department of Energy
by Bechtel Bettis, Inc.

DISCLAIMER

DRY PATCH STABILITY OF SHEAR DRIVEN LIQUID FILM

David G. Penn
Purdue University
dpenn@Bicron.com

Martin A. Lopez de Bertodano
Purdue University
bertodan@ecn.purdue.edu

Paul Lykoudis
Purdue University
lykoudis@ecn.purdue.edu

Stephen G. Beus
Bettis Atomic Power Lab
beussg@bettis.gov

ABSTRACT

The breakdown of the liquid film at the wall in annular gas-liquid flow may lead to the formation of a stable dry patch. For the case of heat transfer surfaces this causes a hot spot. The dry patch is a partial area on the solid surface that is non-wetted due to a local disturbance of the flow and is sustained by surface tension. Dry patch stability is dependent on a balance of body and surface forces. In the present study the interfacial shear force drives the film and the gravity force is negligible.

A new computational fluid dynamics (CFD) solution of the flow field in the film around the dry patch has been obtained. The CFD results confirm Murgatroyd's shear force model (1965), although the details are more complex. Furthermore, there is agreement between the CFD solution and the experimental value of the characteristic length scale, λ, for the shear force.

In addition new experimental data have been taken for adiabatic upward annular air-water and air-ethylene glycol flows at room temperature in a 9.5 mm diameter tube. They provide validation of Murgatroyd's model over a wider range of the film's Reynolds number than previous data.

INTRODUCTION

Hewitt and Lacey (1965) proposed a model for dry patches of shear driven films. It includes inertia, surface tension and gravity but the film contact angle had to be adjusted to a smaller value to fit their experimental data. Murgatroyd (1965) proposed an additional force, caused by unbalanced shear stresses near the dry patch. With this force, which will be referred to as the shear force, the observed value of the contact angle fits the data. Upstream of the dry patch the shear forces at the wall-liquid and liquid-gas interfaces are equal and opposite, assuming gravity is negligible. But near the edge of the dry patch, along the dividing streamline, the wall shear goes to zero whereas the interfacial shear remains the same. The magnitude of the net shear force on the film is determined by a characteristic length, λ, over which this imbalance occurs. However Murgatroyd did not validate the model with a mathematical solution for the distribution of the shear stresses. Instead he determined λ empirically to fit the experimental data. Penn et. al. (1998) obtained a solution of the flow around the dry patch using CFD. This paper is a continuation of that work.

NOMENCLATURE

D	tube diameter
d	dry patch diameter
g	Gravity
l	width of computational domain
M	Momentum flow
Re_{film}	Film Reynolds number, $\frac{\rho_l u_l \delta}{\mu_l}$
u,v,w	Velocities
u_0	Interfacial liquid velocity
δ	Film thickness
θ	Contact angle
σ	Surface tension
λ	Characteristic length
μ	Dynamic viscosity
τ_{sf}	Wall shear
τ_{fg}	Shear at liquid-gas interface
ρ_l	Liquid density
ρ_g	Gas density

ANALYTIC MODEL

The force balance model contains the forces that act on a control volume situated along the center streamline of the liquid film leading to the dry patch. A diagram of the film and the control volume are shown in Figure 1. The liquid film is considered to be symmetric along the dividing streamline (E-G). At point E the liquid film is undisturbed, and has a laminar velocity profile, i.e., Couette flow. Point G is a stagnation point. The liquid film at the edge of the dry patch is characterized by the static liquid-solid contact angle. The gas flow is assumed to produce a uniform shear over the film. This is a good approximation since a typical film thickness is approximately 100 microns, and the resulting change in the gas velocity from the

wetted area to the non-wetted area is very small. Furthermore the effect of the surface waves is neglected.

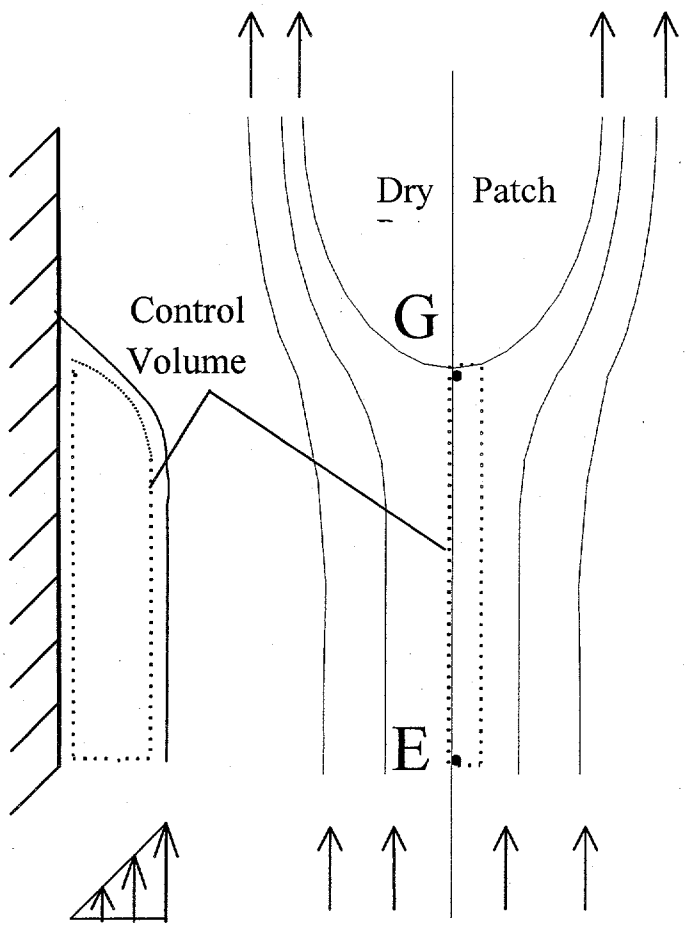

Figure 1 Dry patch schematic

The adiabatic dry patch model contains four components: liquid inertia, gravity, surface tension and the shear force.

The liquid inertia effect is due to the change in fluid momentum entering the control volume at point E and exiting through the right side between points E and G (Figure 1). The fluid enters the control volume fully developed and then curves around the dry patch thus changing its direction and momentum. The inertia "force" per unit width, Δz, is:

$$\frac{F_m}{\Delta z} = \frac{M_{in} - M_{out}}{\Delta z} = \frac{1}{2}\rho_l \int u^2 dy \qquad (1)$$

The Couette flow at the entrance of the control volume is given by,

$$u(y) = \frac{u_0}{\delta} y \qquad (2)$$

where u_0 is the liquid velocity at the liquid-gas interface and δ is the film thickness. Substituting Equation 2 into Equation 1 and integrating across the film thickness yields

$$\frac{F_m}{\Delta z} = \frac{1}{6}\rho_l \delta\, u_0^2 \qquad (3)$$

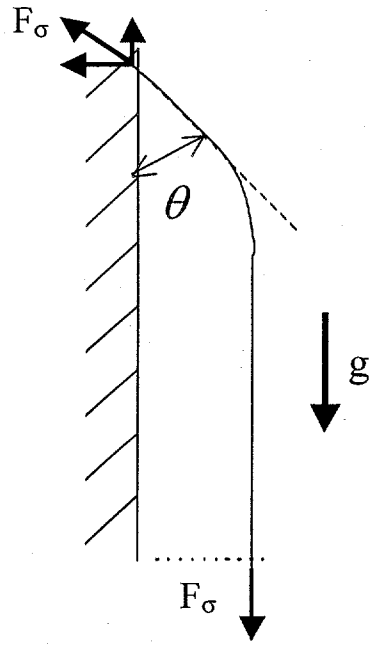

Figure 2 Surface tension force

The net surface tension force on the control volume is caused by the difference in the x direction component of the surface tension at the two ends of the control volume as shown in Figure 2. Thus the net surface tension force per unit width over the control volume is:

$$\frac{F_\sigma}{\Delta z} = \sigma(1 - \cos\theta) \qquad (4)$$

The gravity term for the control volume is simply:

$$\frac{F_g}{\Delta z} = \rho_l g \lambda \delta \qquad (5)$$

where λ is the length of the control volume in the x direction.

The shear force relies on the assumption that the viscous shear at the liquid-solid interface goes to zero at the stagnation point. The shear force at the liquid-gas interface remains constant over the entire area of the control volume.

The unbalance in the shear results from the difference in the shear at the two interfaces. A graphical representation of the shear forces is shown in Figure 3. At point E the shear stresses at both interfaces are equal but in opposite directions (i.e.: fully developed flow). Approaching the dry patch, the shear at the solid wall decreases and the shear at the gas interface remains constant. This produces a net surface force over the control volume. Murgatroyd assumed the wall shear to be a linear function of x:

$$\tau_{sf} = \tau_{fg}\frac{x}{\lambda} \quad for\ x < \lambda \qquad (6)$$
$$\tau_{sf} = \tau_{fg} \quad for\ x \geq \lambda$$

where λ is the characteristic length over which the shear stresses are not in equilibrium. The shear force is obtained integrating the shear stresses over the control volume surface from G to E:

$$\frac{F_\tau}{\Delta z} = \tau_{fg}\int_0^\lambda (1-\frac{x}{\lambda})dx = \tau_{fg}\frac{\lambda}{2} \qquad (7)$$

The shear stress τ_{fg} may be calculated with an interfacial shear model (e.g. Wallis, 1969).
The total force balance on the liquid film is finally the summation of the four separate forces:

$$\frac{1}{6}\rho_l \delta u_{0l}^2 + \frac{1}{2}\lambda\tau_{fg} = \rho_l g\delta\lambda + \sigma(1-\cos\theta) \qquad (8)$$

If the left hand side of equation (8) is dominant then the dry patch will be unstable and will be washed away, if both sides are equal then the dry patch will remain stationary, otherwise the dry patch will grow or move slowly along the solid surface. Equation (8) has an unknown term, λ. In the rest of the paper a relation for it is developed using computational fluid dynamics and experimental data.

One non-dimensional number can characterize adiabatic dry patch stability for a fluid with high surface tension, such as air-water flows, when the surface tension force and shear are dominant. If the ratio of these two forces is greater than one then a dry patch should remain stable, so the stability condition is:

$$\pi_\sigma = \frac{\sigma(1-\cos\theta)}{\frac{1}{2}\lambda\tau_{fg}} > 1 \qquad (9)$$

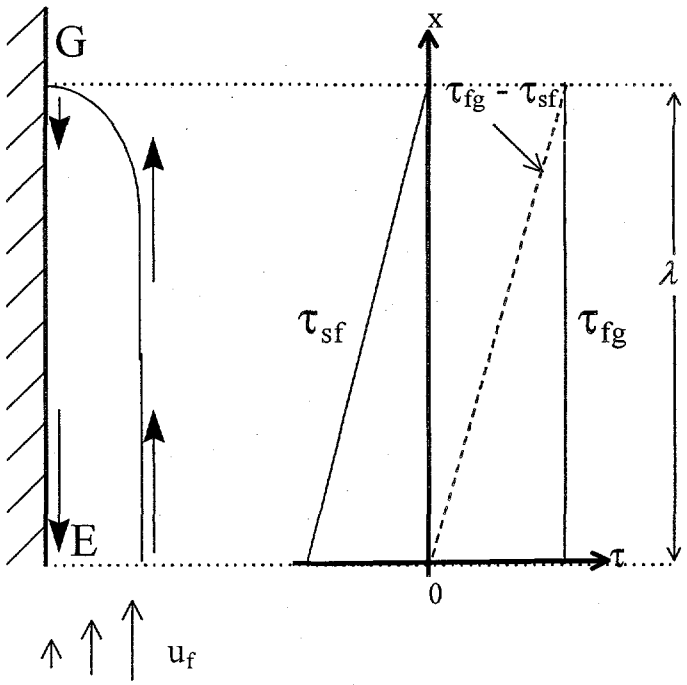

Figure 3. Unbalanced shear stresses acting on the control volume. (τ_{fg} is the stress at the liquid gas interface and τ_{fs} is the stress at the wall)

CFD MODEL

A relation for λ is obtained with the aid of the computational fluid dynamics (CFD) code PHOENICS. The flow field of the liquid film is first calculated to determine the viscous stress field so that λ may be found.

To get an accurate solution the geometry of the CFD model should be close to the actual flow. The control volume used for the CFD model is different from that of the analytic model. The computational domain is shown in Figure 4. The flow domain is 30 mm long and 15 mm wide. The width corresponds to half the circumference of the tube. The depth of the film is 0.1 mm. The dry patch is a semi-circle 20 mm wide. Because of symmetry only half of the dry patch is included in the computational domain.

Figure 4. Body fitted coordinate grid for dry patch CFD simulation.

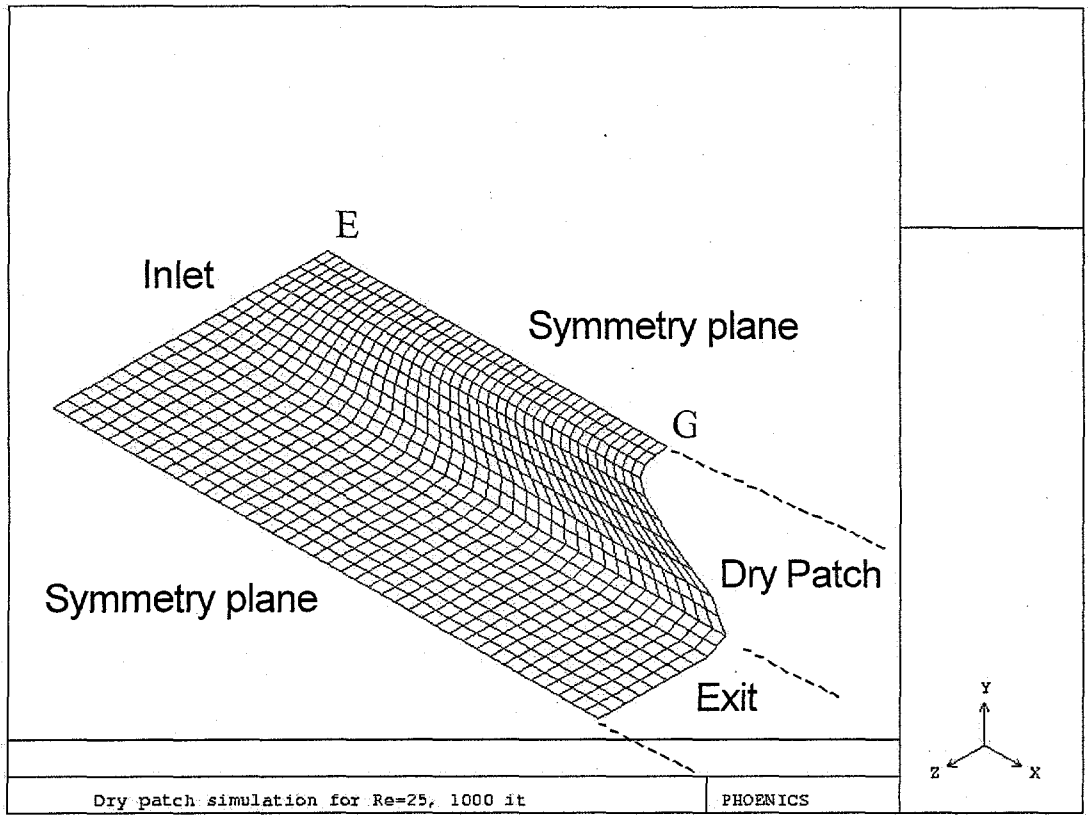

The CFD model is setup so the liquid film has fully developed Couette flow, given by Equation 2, at the inlet and is uniform in the z direction. It is important to note that Equation 2 corresponds to Couette flow without the effect of gravity.

The left side of the liquid film is the center streamline leading to the dry patch. This is a plane of symmetry. The right side of the liquid film is also a plane of symmetry since the width of the grid in the z direction is ½ of the inside diameter of the tube. It is assumed that an actual flow has only one dry patch. The size and shape are similar to observations in the laboratory.

The upper surface of the film is the liquid-gas interface. The boundary condition at this surface is a uniform shear stress in the x direction. The lower surface of the liquid film is the liquid-solid interface. At this interface there is a no-slip boundary condition.

The film flow must turn around the edge of the dry patch. The boundary condition is no flow across this surface, which is assumed perpendicular to the wall for simplicity. The final boundary is the outlet and here there is no restriction imposed. Therefore the fluid can only enter at the inlet and will only leave at the outlet.

The flow slows as it approaches the dry patch and there is a stagnation zone near the point G (Figure 5). In this zone the net flow is stagnant and since the flow in the upper surface of the film is in the positive x-direction because the shear is positive and uniform there, the flow near the wall must be in the negative x-direction. Therefore the flow at the bottom of the film actually reverses near the stagnation point, and so does the shear stress (Figures 6 and 7).

Once the basic flow pattern has been obtained the shear stress distribution along the dividing streamline is calculated. Since the velocity field through the liquid film is known from the CFD solution, and the area of each cell in the mesh is known, the shear force per cell surface area is:

$$F_\tau = -\mu \frac{u_{cell}}{\frac{1}{2}\delta_{cell}} A_{cell}. \qquad (10)$$

where u_{cell} is the velocity in the cell layer adjacent to the wall. Comparing the resulting stress distribution shown in Figure 6 with Figure 3 it is seen that the stress distribution proposed by Murgatroyd is too simple. However the basic idea that the shear stress at the wall goes to zero at the intersection of the dividing streamline and the line of contact of the dry patch is correct.

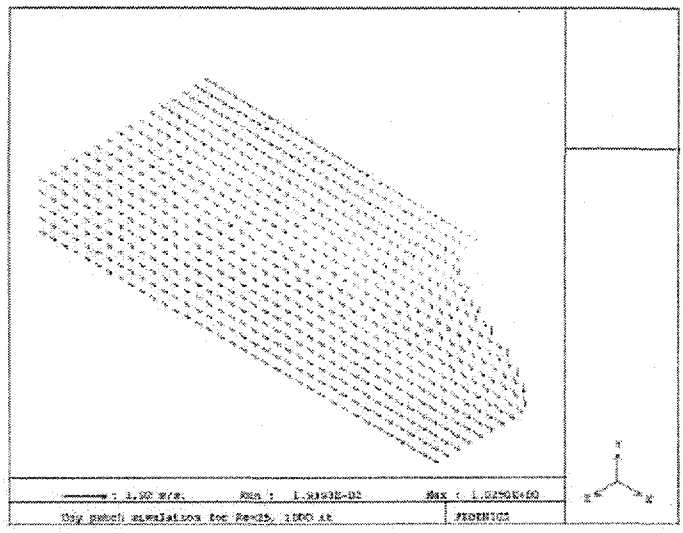

Figure 5 Velocity vectors around the dry patch

The length λ is calculated by integrating the shear stress profile (i.e.: summing the individual cell shear stresses along the dividing streamline) at both interfaces starting from the edge of the dry patch and moving upstream. λ is defined as the distance from the edge of the dry patch to the point where the integrated liquid-solid shear force is ½ of the liquid-gas shear force. This arbitrary definition is used to match Murgatroyd's model (i.e.: Equation 7) .

This calculation of λ was performed for different film Reynolds numbers, where:

$$\mathrm{Re}_{film} = \frac{\rho_l u_l \delta}{\mu_l}. \qquad (11)$$

The solid line in Figure 7 shows the results of the CFD calculations. The change of λ/δ with the film Reynolds number is small which means that the inertia of the fluid has little effect. This is a consequence of the low values of Re over which stable dry patches occur. If dry patches were to occur at higher values of Re then inertial would play a role.

A convergence study was performed on both the number of iterations and the refinement in the mesh spacing.

Three different grids were generated to test mesh refinement convergence, by doubling the number of cells in each direction. The velocity profile at a location 1 mm from the dividing streamline and 1mm away from the dry patch is plotted in Figure 8. This Figure shows that the refinement in the mesh spacing from the 40x10x20 grid to the 80x20x40 grid does not produce a substantially improved solution. This is especially true near the liquid-solid interface where the calculation of λ is made. Based on this result all the calculations were performed with the 40x10x20 grid.

In a similar way the number of iterations was doubled successively until the solution for λ stopped changing.

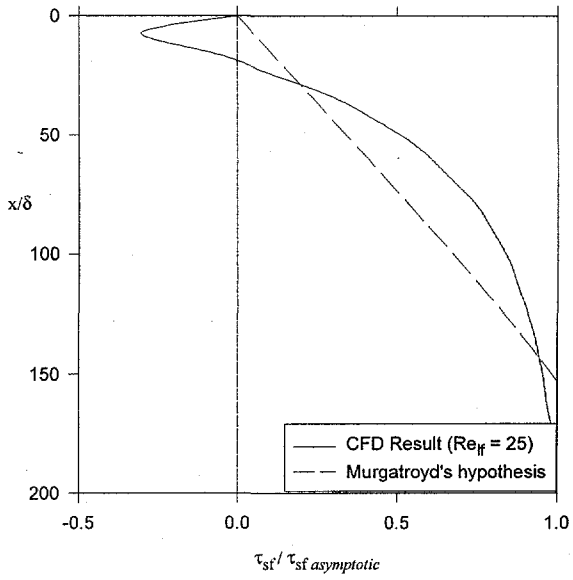

Figure 6 Wall shear stress along the dividing streamline

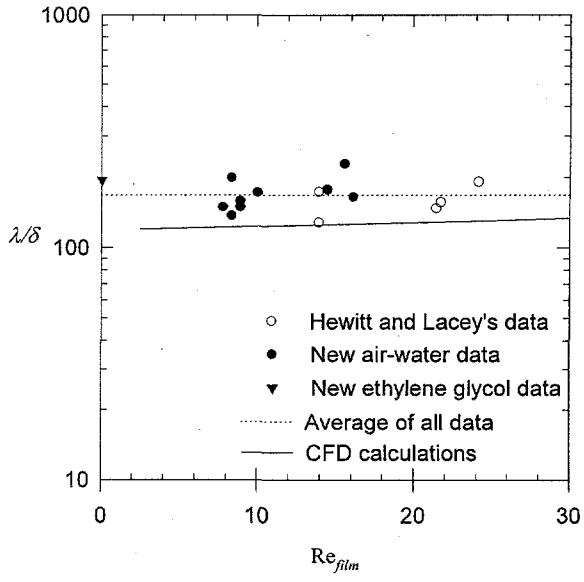

Figure 7 Comparison between model and data

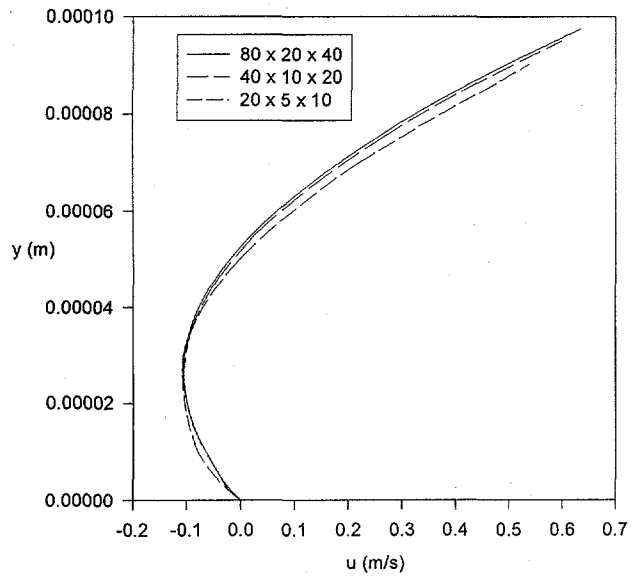

Figure 8 Mesh refinement analysis

SCALING

The objective is to nondimensionalize the Navier Stokes equations and the boundary conditions to find the dimensionless numbers that λ/δ depends on.

The N-S equations for steady state are:

$$\underline{u} \bullet \nabla \underline{u} = -\nabla p + \rho g + \mu \nabla^2 \underline{u} \qquad (12)$$

From the CFD analysis (and from the data) the inertial and gravity terms are negligible so we may simplify the equation as:

$$\nabla p \cong \mu \nabla^2 \underline{u} \qquad (13)$$

where the pressure gradient is sustained by the surface tension and the RHS corresponds to the shear force. In effect if this equation is integrated over the control volume used in the integral analysis the result is the one previously obtained:

$$\sigma(1-\cos\theta) \cong 1/2\ \lambda\tau \qquad (14)$$

And so it is reasonable to nondimensionalize (13) by dividing it by $\sigma(1\text{-}\cos\theta)/\delta^2$,

$$\nabla^* p^* \cong \frac{\mu u_0 \lambda}{\delta\sigma(1-\cos\theta)} \frac{\delta}{\lambda} \nabla^{*2} \underline{u}^* \qquad (15)$$

where $p^* = p/(\sigma/\delta)$ and u_0 is the average velocity of the film far upstream from the dry patch. Also far upstream

$$\tau = \mu \frac{2u_0}{\delta} \qquad (16)$$

Combining (14) and (16) into (15) then yields:

$$\nabla^* p^* \cong \frac{\delta}{\lambda} \nabla^{*2} \underline{u}^* \qquad (17)$$

In a similar way the boundary conditions (c.f.: Figure 4) can be written as:

$$\underline{u}^* = 0 \quad @ \quad y^* = 0 \qquad (18a)$$

$$\frac{\partial u^*}{\partial y^*} = 1, \quad \frac{\partial w^*}{\partial y^*} = 0, \quad v^* = 0 \quad @ \quad y^* = 1 \qquad (18b)$$

$$\underline{u}^* = 2y^* \quad @ \quad x^* = 0 \ (inlet) \qquad (18c)$$

$$\underline{u}^* \bullet \underline{n} = 0 \quad @ \quad \underline{x}^* \in dry\ patch\ strip \qquad (18d)$$

$$\frac{\partial \underline{u}^*}{\partial z^*} = 0 \quad @ \quad z^* = 0, \frac{l}{\delta} (symmetry\ planes) \qquad (18e)$$

$$p^* = 0 \quad @ \quad \underline{x}^* \in exit\ \ strip \qquad (18f)$$

From this analysis the dimensionless groups that appear are λ/δ from (17), d/δ from (18d) and l/δ from (18e) where d is the size of the dry patch and l is the width of the computational domain in the z direction. Then:

$$\frac{\lambda}{\delta} = f\left(\frac{d}{\delta}, \frac{l}{\delta}\right) \qquad (19)$$

EXPERIMENT

The experiment is similar to Hewitt and Lacey's (1965). A vertical air-water loop is used, Figure 9, with a 9.5 mm I.D. test section. In this experiment the annular flow is developed in a mixing chamber at the base of the test section. The mixing chamber consists of a porous tube through which the liquid film is injected. The air flows into the porous tube from the bottom. The liquid and gas flow rates are controlled with fine adjustment needle valves and the flow is monitored using standard rotameters. The test section itself is approximately 300 tube diameters long and constructed of clear 9.5 mm I.D. Lexan tubing. The length of the test section assures that the flow will be fully developed at the measurement area. The system pressure and pressure drop across the test section are measured with mercury and water manometers respectively. The film thickness is measured using a needle attached to the end of a micrometer, the needle is at a 20° angle to the tube wall and it enters the test section downstream of the measurement area so it can contact the film without disturbing the flow upstream.

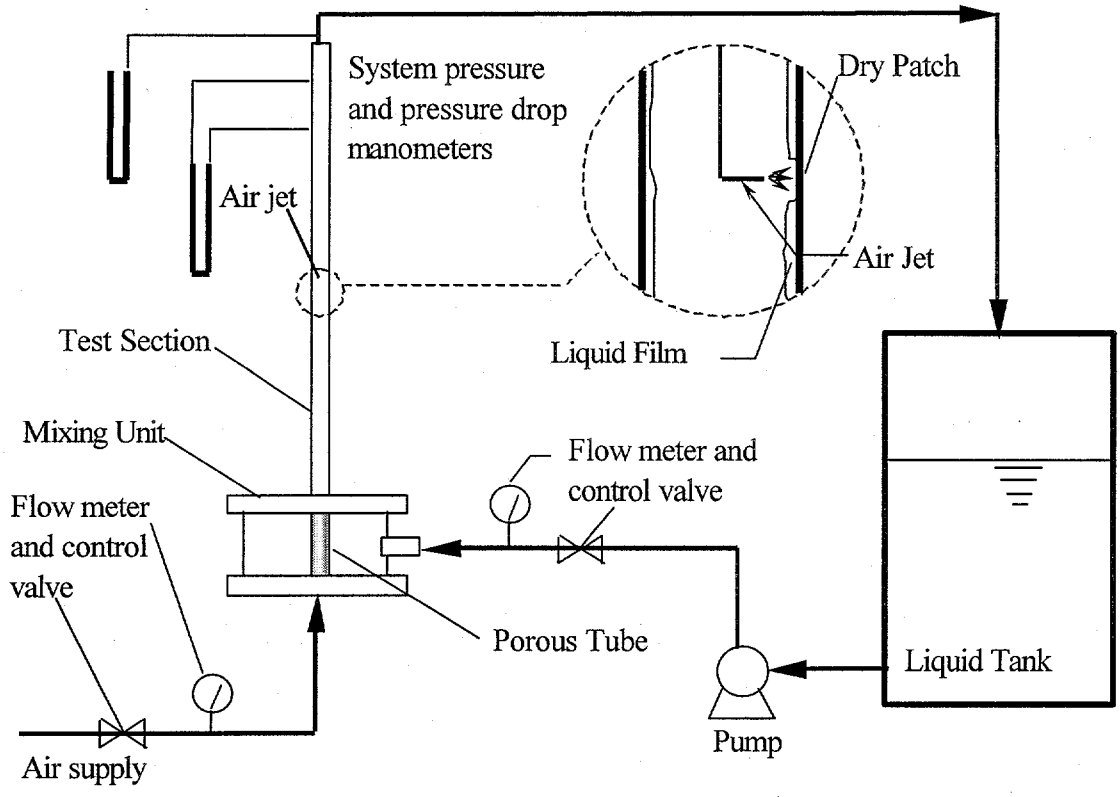

Figure 9 Schematic of experiment

Experiments were carried out with air-water and air-ethylene glycol (properties of water: the surface tension is 0.0735 N/m, the density is 998 kg/m^3 and the viscosity is 1 cp; properties of ethylene-glycol: the surface tension is 0.0484 N/m, the density is 1119 kg/m^3 and the viscosity is 19.9 cp, taken at 20°C from the CRC Handbook of Chemistry and Physics, 50th edition). The values of the wetting angle, θ, were measured separately by placing a liquid drop on a Lexan sheet and taking a close up photography of the profile of the droplet. The measured values for water and ethylene-glycol were approximately 60°. The value for water is in agreement with the data of Chappius (1982).

The dry patch is initiated by creating a disturbance to the flow with a small air jet as shown in Figure 9. An electric solenoid valve and a pressure regulator control the air jet.

At the beginning of the experiment the tube wall is completely wetted with a film and the gas flow is kept at a moderate value to sustain the annular regime (i.e.: j_g is approximately 20 m/s). The liquid flow rate is then reduced and held constant while the gas flow is reduced in small steps to reduce the shear in the film. After each successive reduction of the gas flow the air jet is cycled to create a dry patch. Depending on which forces dominate the flow the dry patch will remain in a stagnant position or the liquid will rewet the surface. If the liquid film will no longer rewet the surface and the dry patch is stagnant then it is considered to be a stable dry patch and the data is recorded.

The experimental data are presented in Table 1 and Figure 7 along with data from the experiment of Hewitt and Lacey (1965). The average value of all the data is $\lambda/\delta = 168$ with a standard deviation of 16% and a maximum deviation of 35%.

The values of λ/δ were calculated such that Equation 8 is satisfied. It is also noted that the shear stress was obtained from the measured pressure drop, and not calculated from the gas velocity. The air-ethylene glycol datum was obtained for further validation of the model at different conditions. Ethylene glycol has a viscosity approximately 20 times smaller than water and the film Reynolds number is two orders of magnitude smaller (c.f.: Table 1).

DISCUSSION

Table 1 contains the new data together with Hewitt and Lacey's. For the air-water experiment spontaneous dry patches were observed (i.e.: without the air jet) at very low liquid flows. These data are recorded in Table 1 but they are not analyzed.

The three forces shown the table are calculated from the measurements. The remaining shear force is obtained by satisfying Equation 8. Finally λ/δ is calculated with Equation 7 given the interfacial shear obtained from the pressure drop

measurement. The most significant forces in Equation 8 for all the data in the table are the shear and the surface tension (i.e., the contributions of the gravity and inertia terms are relatively small).

The magnitude of the inertia force is relatively small for all the air-water data and negligibly small for the ethylene-glycol data. Therefore the new experimental data taken over a wider range of Reynolds numbers than previous data show that the effect of Re is negligible over the range of interest. This is in agreement with the small Reynolds number dependence of the CFD results.

The CFD results validate Murgatroyd's shear force model and the CFD values of λ/δ are similar to the experimental data. It is important to note that the CFD calculations were performed for one arbitrary dry patch size and film thickness and that the results vary for a different choice. A computation was performed reducing the film thickness by a factor of two and the value of λ practically did not change, which means that λ/δ doubled. This means that the dry patch size, d, is a better dimension to scale λ than the film thickness, as may be guessed from equation (19). However this measurement is missing in the present experiment, as well as in Hewitt and Lacey's data. If this information could be incorporated into the model the result would be more general. With this limitation it is remarkable that the scatter of the data in Figure 7 is not greater.

The magnitude of the gravity force was never more than 50% of the surface tension force for any of the air-water data obtained, and in general it was much smaller. This was not true for ethylene glycol where the gravity force was greater than the surface tension force for all the measurements other than the one shown. The model did not work in those cases. Thus another limitation of the present analysis is that the CFD model does not include the effect of gravity, and therefore the dependence of λ on gravity has not been determined. However the method developed in this work could be extended to consider this effect. Based on the experimental results the limit of the present theory may be defined by

$$\pi_g = \frac{\rho_l g \delta}{\frac{1}{2}\tau_{fg}} < 0.5 \qquad (20)$$

If the model is applied to high pressure steam water conditions, where the contact angle and the surface tension are very small, then equation (9) can only be satisfied if the shear becomes negligible. Therefore dry patches produced by surface tension do not appear. This was confirmed in the laboratory with a Freon-113 dry-out visualization experiment (i.e.: Freon-113 also has a very small contact angle). It was not possible to observe any dry patches over a heated test section (with heat fluxes less than 60,000 W/m^2) until the film evaporated completely.

CONCLUSION

Two separate results have been obtained on the stability of dry patches of the shear driven liquid film in annular two-phase flow. The first result is that Murgatroyd's shear force model has been validated using CFD.

The second result are the new experimental data for adiabatic air-water and air-ethylene glycol flows. The length scale needed to correlate the shear force derived from these data is in agreement with the CFD calculations. These data also show that Murgatroyd's model does predict the stability of dry patches over a wide range of Reynolds numbers.

The recommended experimental value for the length scale in Murgatroyd's model is $\lambda/\delta = 168$. This value may be used with Equation 9 to predict stable dry patches for cases where the surface tension force and the shear force are the dominant terms in the force balance.

With these results dry patches may be predicted with the observed contact angle as opposed to a smaller contact angle widely used in the literature. However further work is necessary to obtain a complete model that includes the size of the dry patch.

ACKNOWLEDGMENTS

The financial support of Bettis Atomic Power Laboratory, which made this work possible, is gratefully acknowledged.

REFERENCES

Chappius, J., "Contact Angles," in Multiphase Science and Technology, Eds. G.F. Hewitt, J.M. Delhay, N. Zuber, 1 (1982):387-505.

Hewitt, G.F., D.M.C. Lacey, " The Breakdown of the Liquid Film in Annular Two-phase Flow," International Journal of Heat and Mass Transfer, 8 (1965):781-791.

Murgatroyd, W, " The Role of Shear and Form Forces in the Stability of a Dry Patch on Two-phase Film Flow," International Journal of Heat and Mass Transfer, 8 (1965):297-301.

PHOENICS, CHAM, Bakery House, 40 High Street, Wimbledon Village, London SW19 5AU, United Kingdom.

Penn, D. G., Lopez de Bertodano, M. A., Lykoudis, P. S. and Beus, S. G., "Dry Patch Stability in Adiabatic Annular Flow," 1998 ANS Winter Annual Meeting, Washington, DC, November 15-19, 1998.

Wallis, G. B., "One-dimensional Two Phase Flow", McGraw-Hill, New York, 1969.

Table 1: Dry patch data (Measurements obtained at standard temperature and pressure).

Run	Notes	J_l m/s	J_g m/s	Shear Pa	Film height m	Re_{film}	F inertia N/m	F gravity N/m	F sigma N/m	λ/δ
	Air-water									
1	stationary	0.00655	24.7	5.11	7.81E-05	15.60	0.00208	0.01360	0.03379	227
2	spontaneous	0.00176	25.3	4.09	4.52E-05	4.18				
3	stationary	0.00679	28.1	6.86	6.86E-05	16.16	0.00254	0.00762	0.03379	165
4	spontaneous	0.00164	29.3	4.82	4.02E-05	3.90				
5	stationary	0.00608	28.6	6.72	6.57E-05	14.49	0.00213	0.00749	0.03379	177
6	spontaneous	0.00164	27.0	5.70	3.70E-05	3.90				
7	stationary	0.00351	31.2	8.18	4.52E-05	8.36	0.00103	0.00399	0.03379	199
8	spontaneous	0.00164	31.2	7.16	3.30E-05	3.90				
9	stationary	0.00421	32.5	8.91	4.75E-05	10.03	0.00141	0.00380	0.03379	172
10	spontaneous	0.00164	32.5	8.62	3.01E-05	3.90				
11	stationary	0.00374	35.0	10.95	4.04E-05	8.92	0.00131	0.00252	0.03379	158
12	spontaneous	0.00164	36.0	9.64	2.85E-05	3.90				
13	stationary	0.00374	36.2	12.12	3.84E-05	8.92	0.00138	0.00215	0.03379	149
14	spontaneous	0.00164	36.2	10.81	2.69E-05	3.90				
15	stationary	0.00328	37.8	13.58	3.39E-05	7.80	0.00120	0.00168	0.03379	149
16	spontaneous	0.00211	37.8	13.29	2.75E-05	5.02				
17	stationary	0.00351	37.9	14.75	3.37E-05	8.36	0.00138	0.00152	0.03379	137
18	spontaneous	0.00187	46.5	13.00	2.62E-05	4.46				
2	ethylene glycol	0.00027	37.2	4.71	7.37E-05	0.04	0.00000	0.01146	0.02225	194
27	Hewitt's' data	0.00305	20.1	5.12	9.71E-05	24.17	0.00401	0.01768	0.03379	191
28	Hewitt's' data	0.00274	22.7	6.24	8.35E-05	21.77	0.00378	0.01067	0.03379	156
36	Hewitt's' data	0.00270	22.7	6.63	8.05E-05	21.47	0.00382	0.00934	0.03379	147
47	Hewitt's' data	0.00176	25.7	7.09	6.27E-05	13.94	0.00207	0.00667	0.03379	173
58	Hewitt's' data	0.00176	30.3	10.56	5.14E-05	13.94	0.00252	0.00331	0.03379	128